7. H. S. Cheng and B. Sternlicht, "A numerical solution for the pressure, temperature, and film thickness between two infinitely long lubricated rolling and sliding cylinders under heavy loads," Trans. ASME, Ser. D. J. Basic Eng., 87, No. 3 (1965).

AN EXPERIMENTAL AND THEORETICAL INVESTIGATION OF THE STABILITY OF A LINEAR VORTEX WITH A DEFORMED CORE

V. A. Vladimirov, L. Ya. Rybak, and V. F. Tarasov

UDC 532.527+532.516

Experiments and a mathematical model of the instability of a linear vortex subject to deformation such that the streamlines are nearly ellipses with small eccentricities are described in the report. The tests were carried out with a draining-vortex type of flow in a cylindrical vessel with an elliptical cross section. The wavelengths and rotation rates of unstable modes were measured. An analytical model of the instability is proposed, based on linear theory using perturbation theory relative to the smallness of the deformation. According to this model, the mechanism of the observed instability is analogous to the instability of a wave of finite amplitude in a three-wave interaction [1, 2]. The predictions of the model explain the experimental results fairly well.

These tests can be considered as a generalization of the experiments of [3, 4] on the stability of initially rigid-body rotation inside an elliptical cylinder after it is stopped. The proposed theory of the phenomenon can also be considered as a generalization of that of [5], in which the question of the stability of a linear vortex in an unbouded fluid was investigated. The core of the vortex was assumed to be subject to deformation such that the shape of its cross section is close to an ellipse with a small eccentricity. The method of solution of [5] is used below. A theory for the above-mentioned experiments was constructed in [3, 4] on the basis of the assumption that the vorticity is constant. In contrast to the present work, Galerkin's method was used. Thus, the results of [3-5] comprise two different limiting cases of the problem under consideration.

1. Let us consider the plane stationary flow of an ideal fluid, consisting of a linear vortex with a core of constant vorticity, which is inside a cylindrical vessel. Outside the core the flow is potential. The shapes of streamlines and of the boundary of the normal cross section of the vessel differ little from circles. The quantity $\varepsilon \ll 1$ serves as the measure of this difference. In the cylindrical coordinate system (r, θ, z) we assign the flow in the form of expansions in powers of the parameter ε,

$$\left.\begin{aligned} U(r,\theta) &= -\varepsilon r\sin 2\theta + O(\varepsilon^2),\\ V(r,\theta) &= r - \varepsilon r\cos 2\theta + O(\varepsilon^2),\\ P(r,\theta) &= (1/2)r^2 + O(\varepsilon^2), \end{aligned}\right\} 0 < r \leqslant R_1(\theta),$$
$$\Phi(r,\theta) = \theta - (\varepsilon/4)(r^2 - r^{-2})\sin 2\theta + O(\varepsilon^2),\ R_1(\theta) \leqslant r \leqslant R_2(\theta), \tag{1.1}$$

where $R_1(\theta)$ and $R_2(\theta)$ give the boundaries of the vorticity core and the vessel,

$$\begin{aligned} R_1(\theta) &= 1 + (\varepsilon/2)\cos 2\theta + O(\varepsilon^2),\\ R_2(\theta) &= b[1 + (\varepsilon/4)B\cos 2\theta + O(\varepsilon^2)]. \end{aligned} \tag{1.2}$$

The radial and angular components of the velocity and pressure inside the vorticity core are designated as U, V, and P; Φ is the velocity potential outside this core; b is a constant equal to the vessel raidus in the zeroth approximation ($b \geqslant 1$); $B = b^2 + b^{-2}$. A system of units is used in which the vorticity in the core equals zero while the unperturbed radius of the core equals one. The first two terms of the expansion of the exact solution obtained in [6] (cited in [5]) are written out explicitly in (1.1) and (1.2). These expansions can also be obtained by a direct solution of the equations of motion by successive approximations satisfying the conditions of nonpenetration at $r = R_2(\theta)$.

Novosibirsk. Translated from Zhurnal Prikladnoi Mekhaniki i Tekhnicheskoi Fiziki, No. 3, pp. 61-69, May-June, 1983. Original article submitted May 12, 1982.

0021-8944/83/2403-0337$07.50

If terms of order ε^2 and higher are discarded, the form of the function $R_2(\theta)$ coincides with the analogous representation for an ellipse with a small eccentricity. Let a_0 and b_0 ($a_0 > b_0$) be the semiaxes of this ellipse. Then

$$b^2 = 2a_0^2b_0^2/(a_0^2 + b_0^2), \quad \varepsilon = \frac{2\varepsilon_0}{B}, \quad \varepsilon_0 \equiv \frac{a_0^2 - b_0^2}{a_0^2 + b_0^2}. \tag{1.3}$$

We note that the smallness parameter ε_0 is determined only by the vessel geometry, while ε is also determined by the ratio b of sizes of the vessel and the vortex core.

Let us turn to the formulation of the problem of the stability of the flow (1.1), (1.2). The behavior of infinitely small perturbations is described by the linearized system of equations of motion. For the region inside the vorticity core these equations have the form

$$\begin{gathered} Lu + \frac{\partial U}{\partial r}u + \frac{1}{r}\frac{\partial U}{\partial \theta}v - \frac{2Vv}{r} = -\frac{\partial p}{\partial r}, \\ Lv + \frac{\partial V}{\partial r}u + \frac{1}{r}\frac{\partial V}{\partial \theta}v + \frac{1}{r}(Uv + Vu) = -\frac{1}{r}\frac{\partial p}{\partial \theta}, \\ Lw = -\frac{\partial p}{\partial z}, \frac{\partial u}{\partial r} + \frac{u}{r} + \frac{1}{r}\frac{\partial v}{\partial \theta} + \frac{\partial w}{\partial z} = 0, \end{gathered} \tag{1.4}$$

and for the region outside the core

$$\Delta\varphi = 0. \tag{1.5}$$

The fields of perturbations of the r, θ, and z components of the velocity, the pressure, and the velocity potential are designated as u, v, w, p, and φ, while $L \equiv \partial/\partial t + U\partial/\partial r + (1/r)V\partial/\partial\theta$. The boundary conditions for the perturbations are under the requirement of nonpenetration at $r = R_2(\theta)$, the absence of singularities at $r = 0$, and the fulfillment of the kinematic and dynamic conditions at the boundary between the vorticity core and the potential stream. The form of these conditions is cumbersome and is not given in the present article.

Using the independence of the main flow (1.1) from z and t, we take

$$(u, v, w, p, \varphi) = (u_a, v_a, w_a, p_a, \varphi_a)e^{\omega t + ikz} \tag{1.6}$$

with the amplitudes u_a, v_a, w_a, p_a, and φ_a dependent only on r and θ. After substituting (1.6) into (1.4), (1.5), and the boundary conditions, we obtain the problem of determining the amplitude and the eigenvalues ω. If there exists at least one ω with Re $\omega > 0$, then the flow is unstable.

2. In the formulated statement the problem of determining the eigenvalues ω is very complicated and will be solved by the method of successive approximations using the smallness of ε. The calculations are made for the zeroth and first approximations.

Presuming solutions through analytical functions of ε (in the vicinity of $\varepsilon = 0$), we write them in the series from ($\nu = 0, 1, 2, \ldots$)

$$(u_a, v_a, w_a, p_a, \varphi_a, \omega) = \sum_{\nu=0}^{\infty} \varepsilon^{\nu}(u_\nu, v_\nu, w_\nu, p_\nu, \varphi_\nu, \omega_\nu). \tag{2.1}$$

In addition, we set $k = k_0 + \varepsilon k_1$. The latter representation was adopted because the quantity k_0 satisfies a certain set of dispersion relations, and cases of instability will correspond to a discrete set of values of k_0. The quantity k_1 allows us to consider values of k close to k_0. Substituting (2.1) into (1.4) and equating terms with equal powers of ε yields

$$\left.\begin{aligned} &L_0u_\nu - 2v_\nu + \frac{\partial p_\nu}{\partial r} = G_{1\nu}, \\ &L_0v_\nu + 2u_\nu + \frac{1}{r}\frac{\partial p_\nu}{\partial \theta} = G_{2\nu}, \\ &L_0w_\nu + ik_0p_\nu = G_{3\nu}, \\ &\frac{\partial u_\nu}{\partial r} + \frac{u_\nu}{r} + \frac{1}{r}\frac{\partial v_\nu}{\partial \theta} + ik_0w_\nu = G_{4\nu}, \end{aligned}\right\} 0 < r < 1, \tag{2.2}$$

$$\frac{\partial^2\varphi_\nu}{\partial r^2}+\frac{1}{r}\frac{\partial\varphi_\nu}{\partial r}+\frac{1}{r^2}\frac{\partial^2\varphi_\nu}{\partial\theta^2}-k_0^2\varphi_\nu=G_{5\nu},\quad 1<r<b.$$

Here $L_0 \equiv -\omega_0 + \partial/\partial\theta$. For $\nu = 0$ the right sides $G_{l0} = 0$ equal zero for all l ($l = 1, 2, 3, 4, 5$). In equations of the first approximation ($\nu = 1$) G_{l1} contain linear functions of the zeroth approximation, while for $l = 1, 2, 3$ they also contain the quantity ω_1 linearly:

$$G_{11} \equiv \omega_1 u_0 + (r\partial u_0/\partial r + v_0)\sin 2\theta + (\partial u_0/\partial\theta)\cos 2\theta.$$

The kinematic and dynamic boundary conditions at r = 1 for the zeroth and first approximations have the form

$$\frac{\partial\varphi_0}{\partial r}-u_0=0,\quad p_0+\omega_0\varphi_0+\frac{\partial\varphi_0}{\partial\theta}=0,$$

$$\frac{\partial\varphi_1}{\partial r}-u_1=\left(-\frac{\partial\varphi_0}{\partial\theta}+v_0\right)\sin 2\theta+\frac{1}{2}\left(-\frac{\partial^2\varphi_0}{\partial r^2}+\frac{\partial u_0}{\partial r}\right)\cos 2\theta, \tag{2.3}$$

$$p_1+\omega_0\varphi_1+\frac{\partial\varphi_1}{\partial\theta}=-\omega_1\varphi_0+\frac{\partial\varphi_0}{\partial r}\sin 2\theta+\frac{1}{2}\left(2\frac{\partial\varphi_0}{\partial\theta}-\omega_0\frac{\partial\varphi_0}{\partial r}-\frac{\partial^2\varphi_0}{\partial r\partial\theta}-\frac{\partial p_0}{\partial r}\right)\cos 2\theta.$$

The condition of nonpenetration at the cylinder boundary at r = b leads to the conditions

$$\frac{\partial\varphi_0}{\partial r}=0,\quad \frac{\partial\varphi_1}{\partial r}=-\frac{B}{2}\left[\frac{b}{2}\cos 2\theta\frac{\partial^2\varphi_0}{\partial r^2}+\frac{1}{b}\sin 2\theta\frac{\partial\varphi_0}{\partial\theta}\right], \tag{2.4}$$

which are "displaced" as usual from the true boundaries (1.2) to the close vicinities of them, r = 1 and r = b. One more condition consists in the finiteness of the solutions of any approximation at r = 0.

3. Let us consider the problem (2.2)-(2.4) of the zeroth approximation. Its solutions consist of inertial waves on a linear vortex with a circular core of constant vorticity. The vessel boundary is the circle r = b. These waves with b = ∞ were studied long ago by Kelvin [7]. For the harmonic proportional to $e^{im\theta}$, from (2.2) we obtain

$$\begin{aligned} p_0 &= \beta J_m(\eta_m r)e^{im\theta} \quad \text{for} \quad 0<r<1,\\ \varphi_0 &= \alpha\Psi_m(k_0 r)e^{im\theta} \quad \text{for} \quad 1<r<b, \end{aligned} \tag{3.1}$$

where $\Psi_m(x) \equiv K_m(x) - \varkappa_m I_m(x)$; $\varkappa_m \equiv K_m'(k_0b)/I_m'(k_0b)$; $K_m'(x) \equiv dK_m(x)/dx$; J_m, N_m, K_m, and I_m are Bessel, Neumann, and modified Bessel functions of index m; α and β are complex constants; $\eta_m^2 \equiv -k_0^2\Delta_m/\sigma_m^2$; $\Delta_m \equiv \sigma_m^2 + 4$; $\sigma_m \equiv \omega_0 + im$. The boundary condition at r = b and the absence of singularities at r = 0 are taken into account in (3.1). Drawing upon the boundary conditions (2.3) at r = 1 yields the dispersion relation between ω_0 and k_0,

$$k_0 J_m\Psi_m'(k_0)-\frac{\sigma_m}{\Delta_m}\Psi_m(k_0)\left[\sigma_m\eta_m J_m'+2imJ_m\right]=0, \tag{3.2}$$

where $J_m \equiv J_m(\eta_m)$. The constants α and β also prove to be connected. One can show that the spectrum of $i\omega_0$ given by (3.2) is real and $m - 2 < i\omega_0 < m + 2$.

4. For the problem (2.2)-(2.4) of the first approximation the form of the solutions and the value of ω_1 can be obtained using simple but cumbersome calculations. Their meaning comes down to the determination of corrections to the inertial waves (3.1) due to the difference from circular geometry. The most complicated step is the solution of the inhomogeneous equations (2.2). Since analogous calculations were made in [5] for the case of b = ∞, we present the results without dwelling on them.

If the zeroth approximation is chosen in the form of the harmonic (3.1) with any m, then the quantity ω_1 is always purely imaginary. This corresponds to stability in the first approximation. More significant is the case of degeneration, when the perturbation of the

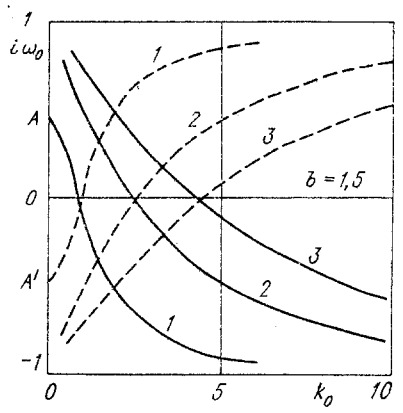

Fig. 1

zeroth approximation, characterized by a frequency ω_0 and a wave vector k_0, has the form of a superposition of several modes with different m (m_1 and m_2). For this case it is shown that if $m_1 - m_2 \neq \pm 2$, then ω_1 is again purely imaginary. Instability (Re $\omega_1 > 0$) can occur only for $m_1 - m_2 = \pm 2$. This result is a consequence of the angular dependence (1.1) of the main flow appearing in the first parts of (2.2). From the form of the spectrum of the problem in the zeroth approximation of Sec. 3 it follows that degeneration can only be two-fold in this case and "dangerous" perturbations in the zeroth approximation have the form

$$p_0 = \beta J_{n+1}(\eta_{n+1}r)e^{i(n+1)\theta} + \bar{\beta} J_{n-1}(\eta_{n-1}r)e^{i(n-1)\theta},$$
$$\varphi_0 = \alpha \Psi_{n+1}(k_0 r)e^{i(n+1)\theta} + \bar{\alpha} \Psi_{n-1}(k_0 r)e^{i(n-1)\theta}. \tag{4.1}$$

Here the functions p_0 and φ_0 are determined at $0 < r < 1$ and $1 < r < b$, respectively; α, $\bar{\alpha}$, β, and $\bar{\beta}$ are complex constants; a bar above denotes an independent quantity rather than the complex-conjugate operation; n is an arbitrary integer.

Below we shall study instability only on the analytically simplest example of n = 0. This case corresponds to perturbations with bending of the axis of rotation and is the most important from the aspect of experimental practice. Results for $n \neq 0$ in the case of b = 1 are presented in [8]. Let us make several comments about the values of (ω_0, k_0) for which degeneration (4.1) is possible. The dispersion relations for the harmonics appearing in (4.1) for n = 0 are given by the substitution of $m = \pm 1$ into (3.2). By virtue of the degeneration, we consider the points of intersection of the curves (3.2) with m = 1 and $m = -1$ in the plane of k_0 and $i\omega_0$. The intersecting families of these curves are concentrated in the band of $-1 < i\omega_0 < 1$; their appearance for b = 1.5 is presented in Fig. 1. The solid lines correspond to the harmonic m = 1 and the dashed lines to the harmonic $m = -1$. Only the first three of the calculating set of curves for each harmonic are presented in Fig. 1; the numbers of the curves correspond to the numbers of nulls of the function $u_0(r)$ over $0 < r \leqslant b$. Each point of intersection is designated by a pair of integers (q; s) corresponding to the numbers of intersecting curves of the families m = 1 and $m = -1$. As in [8], points with q = s are called principal points of intersection and points with $q \neq s$ are called side points of intersection. The curves for $m = \pm 1$ are obtained from each other by reflection relative to the axis $i\omega_0 = 0$, so that the principal points of intersection lie on this axis. The points of the null curves corresponding to plane perturbation fields ($k_0 \to 0$) are designated as A and A' in Fig. 1. The distance from A and A' to the origin of coordinates is $1/b^2$. For $b = \infty$ these curves emerge from the point $i\omega_0 = 0$, $k_0 = 0$ and for b = 1 they emerge from the points $i\omega_0 = \pm 1$, $k_0 = 0$. A list of the coordinates of the points of intersection for b = 1, 1.2, 1.5, 2, 4, and 6 is given in Table 1, in each cell of which the upper number gives the value of $i\omega_0$ and the lower gives the value of k_0.

Calculations of the quantity ω_1 at the points of degeneration ($i\omega_0$, k_0) yield

$$\omega_1 = -\frac{1}{2} k_0 k_1 (c + \bar{c}) \pm \sqrt{\omega_{\max}^2 + \left[\frac{1}{2} k_0 k_1 (c - \bar{c})\right]^2}, \tag{4.2}$$

where $c \equiv g/f$; $\bar{c} \equiv \bar{g}/\bar{f}$; $\omega^2_{\max} \equiv h\bar{h}/f\bar{f}$; the various functions of the quantities $i\omega_0$, k_0, and b, the form of which is given in the Appendix, are designated as f, $\bar{f}$, g, $\bar{g}$, h, and $\bar{h}$. It follows from (4.2) that instability (Re $\omega_1 > 0$) can occur if

TABLE 1

Points of intersection \ b	1	1,2	1,5	2	4	6
(1; 1)	0,0 1,579	0,0 1,245	0,0 0,878	0,0 0,573	0,0 0,229	0,0 0,140
(2; 2)	0,0 3,286	0,0 2,761	0,0 2,552	0,00 2,508	0,0 2,505	0,0 2,505
(3; 3)	0,0 5,061	0,0 4,457	0,0 4,356	0,0 4,349	0,0 4,349	0,0 4,349
(1; 2)	0,292 2,203	0,297 1,789	0,342 1,488	0,386 1,324	0,406 1,264	0,406 1,264
(1; 3)	0,435 2,630	0,449 2,185	0,495 1,907	0,522 1,778	0,528 1,750	0,528 1,750
(2; 3)	0,165 4,046	0,174 3,481	0,185 3,323	0,186 3,301	0,187 3,300	0,187 3,300

TABLE 2

Points of intersection \ b	1	1,2	1,5	2	4	6
(1; 1)	0,531 0,958	0,522 0,811	0,506 0,748	0,502 0,781	0,529 1,157	0,548 1,576
(2; 2)	0,554 2,325	0,549 2,045	0,556 2,047	0,567 2,122	0,571 2,145	0,571 2,145
(3; 3)	0,559 3,701	0,560 3,409	0,567 3,487	0,569 3,517	0,569 3,518	0,569 3,518
(1; 2)	0,111	0,059	0,004	0,014	0,003	0,004
(1; 3)	0,114	0,043	0,001	0,001	0,004	0,004
(2; 3)	0,161	0,033	0,005	0,007	0,007	0,007

$$\omega_{\max}^2 > -[(1/2)\,k_0 k_1 (c-\bar{c})]^2.$$

Since c and $\bar{c}$ are purely imaginary quantities, the largest growth decrement $\omega_1 = \omega_{max}$ is reached for $k_1 = 0$. In this case the following interval of wave numbers proves unstable:

$$|k_1| < k_{\max} \equiv |2\omega_{\max}/(k_0(c-\bar{c}))|. \tag{4.3}$$

The value of $|k_1| = k_{max}$ corresponds to the boundary of the instability region at which Re $\cdot$ $\omega_1 = 0$. The values of ω_{max} at all the points of intersection present in Fig. 1 are presented in Table 2. For the principal points of intersection the upper number in each cell of the table gives the value of ω_{max} and the lower number gives k_{max}. It is seen that all the points of intersection correspond to unstable modes. At the same time, the growth decrements at the principal points of intersection ($i\omega_0 = 0$) are one to two orders of magnitude larger than at the side points. On the basis of (4.3) the same thing can be said about the widths k_{max} of the instability zones. On this basis, observations of nonrotating disturbances ($i\omega_0 = 0$) should be expected in the experiments.

The instability corresponding to the point of intersection (1; 1) proves to be the most important in the experiments. In Fig. 2 we present the dependence on b of the half-wavelength $\lambda \equiv \pi/k_0 b$, the width $\lambda_{max} \equiv (2k_1/k_0 B)\lambda$ of the zone of unstable wavelengths, and the growth decrement ω_{max} at this point. Here the lengths are normalized to the quantity b, i.e.,

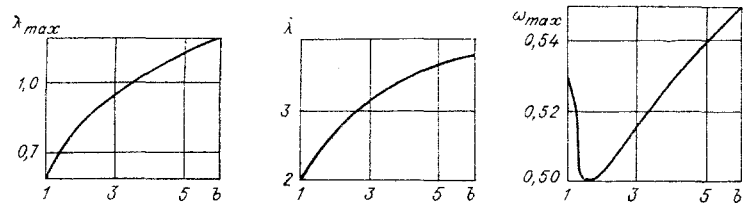

Fig. 2

they are measured in units of the unperturbed vessel radius; λ_{max} is defined so that unstable modes lie in the interval from $\lambda - \varepsilon_0\lambda_{max}$ to $\lambda + \varepsilon_0\lambda_{max}$ [see (1.3)]. Since $\omega_{max} \approx 0.5$ for $1 < b < 6$ (see Fig. 2), the real decrement $\varepsilon\omega_{max} = (2\varepsilon_0/B)\omega_{max}$ decreases as $1/b^2$ as b increases. We also note that $k_0 \to 0$ as $b \to \infty$. In this case the wavelength λ does not approach a finite limit but grows slowly but without limit, so that $\varkappa_1 \approx \ln k_0 - 1/4$ [see (3.1)].

5. A number of tests were made on recording the described instability. We used an installation consisting of a water-filled, round, cylindrical vessel 120 cm high and 18 cm in diameter, placed on a revolving table. Rotation takes place about the axis of symmetry. A rigidly fastened insert in the form of a thin-walled elliptical cylinder made from a thin celluloid sheet was placed inside the vessel. The major axis of the ellipse with a length $2a_0$ coincided with the vessel diameter while the minor axis was varied in the range of $2b_0$ = 13.5-17 cm. The flow inside the elliptical cylinder was observed through the transparent walls. A typical experiment had the following look. The vessel containing water, filled to the level L + δL, was set into a state of rigid-body rotation with a velocity Ω. Then a hole with a diameter d located at the center of the bottom of the vessel was opened. The forming linear vortex (like a vortex in a bath) was made visible by the introduction of dye. When the level fell to the height L the hole was covered and after a time Δt the vessel was abruptly stopped. The interval Δt was needed to reorganize the flow from a draining vortex to a linear vortex with a zero axial velocity component. After stopping, the vortex remains straight in certain ranges of L, while in others one observes instability of the bending type (Fig. 3). Two parameters of an unstable mode were recorded — its rotational velocity $i\omega_0$ and length λ. We present the results of a series of tests with Ω = 0.625 rps, $\varepsilon_0 \approx 0.17$, δL = 15 cm, d = 3 mm, and Δt = 2 sec.

The sequence of pictures in Fig. 3 corresponds to times of 0, 12, and 25 sec after stopping with L = 90 cm. Pictures of the instability for different L (50, 80, and 92 cm) are given in Fig. 4. It was found that in all cases the bends in the vortex core are at rest in the laboratory coordinate system, only varying in amplitude. This corresponds to $i\omega_0 = 0$, i.e., just the case of the principal points of intersection (see Sec. 4). Slight differences of $i\omega_0$ from zero were observed only for bends of large amplitude, when the vortex core almost touched the vessel walls. The results of measurements of the ranges of L for unstable modes are given in the left half of Fig. 5. The hatched sections give the values of L/b in which instability is observed. Each instability zone is designated by a number n_0 = 1, 2, 3, 4 corresponding to a harmonic $n_0\lambda$. A half-wave is observed for n_0 = 1, a whole wave for n_0 = 2, etc. Data of [3, 4] on the instability of initially rigid-body rotation after stopping a vessel with the same ε_0 are presented in the right half of Fig. 5 for comparison.

Direct measurements of the radius a of the vortex core and the vorticity Ω_c in it for this series of tests give values of $a \approx 2$ cm and $\Omega_c \approx 34$ 1/sec. The measurement methods consisted in recording the motion of particles at the free surface and the coloring of the core. The instability zones (1; 1) theoretically predicted for these parameters are plotted on the L/b axis (see Fig. 5) with heavy line segments (n_0 = 1), 2, 3). It is seen that the theory correctly reflects the main result of these tests, consisting in an increase in the wavelengths λ of unstable modes compared with the case of initially rigid-body rotation [3, 4]. At the same time, the theoretically predicted value of λ (see Fig. 5) is somewhat larger than the measured value, while the width λ_{max} of the instability zone is somewhat smaller.

Tests were also made with other values of the parameters ε_0, d, Ω, δL, and Δt. The results obtained are similar to those presented. The instability is manifested more and more weakly with changes in these parameters resulting in an increase in b. In theory this

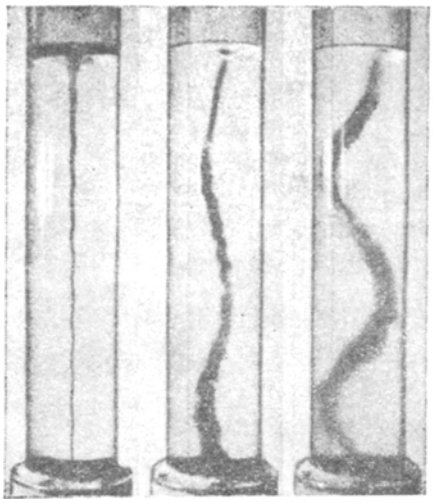

Fig. 3

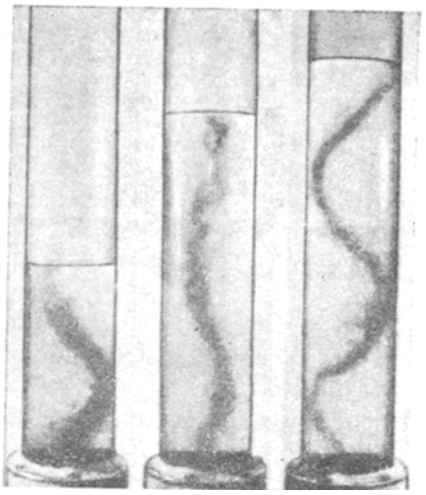

Fig. 4

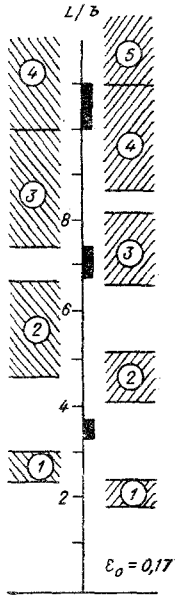

Fig. 5

corresponds to a decrease in the growth decrement $\varepsilon\omega_{max} \sim 1/b^2$. In tests with $b \gtrsim 10$ there is no instability at all.

Let us make several more comments.

1. The growth decrement is almost the same for all the principal points of intersection. To explain the dominant role of the (1; 1) instability one must evidently resort to nonlinear theory. The nonlinear restrictions for the other instabilities corresponding to principal points are intuitively clear: For them to occur the vortex lines in neighboring cylindrical layers must turn in opposite directions, whereas the (1; 1) instability yields a turning of the axis of rotation for the entire flow as a whole.

2. Calculations of the shifts in the principal points of intersection of the dispersion curves show that the difference between theory and experiment can be explained by the nonpotential nature of the flow surrounding the core occurring in the experiments. Allowance for its nonpotential nature evidently also results in the observed broadening of the instability zones.

3. The above model can explain the deviations of the theoretical predictions of wavelengths of unstable modes from the experimental results which occur in [3, 4]. For this one must consider that stopping the vessel results in the rapid reorganization of the velocity profile through turbulent mixing caused by centrifugal instability. Therefore, a constant

vorticity occurs not in the entire flow but only in some core of it, outside of which the vorticity is considerably lower. Such flow reorganization can only result in an increase in λ (see Fig. 2), which is needed to achieve agreement in [3, 4].

4. The experimental setup differs from the theoretical model of Secs. 1 and 2 by the presence of a free surface. Control tests with a rigid cover showed that, at least for a setup like that of [3, 4] with initially rigid-body rotation, in the range of 0.25 rps < Ω < 1.25 rps the influence of the free surface on the instability parameters was weak.

5. The extraneous operation of covering the hole is present in the experimental setup. It was performed to satisfy the assumption (Sec. 1) that the axial velocity component of the main flow equals zero. When the vessel is stopped without covering the hole one also observes instability of the draining vortex like that presented in Figs. 3 and 4. A more complicated theory is needed there, however.

APPENDIX

The following representations are valid for side points of intersection ($i\omega_0$, k_0):

$$f \equiv -A\Psi - H_1\Psi_r + \frac{\sigma}{\Delta}\Psi\left[-\eta\left(\sigma^2 + \frac{8i}{\sigma}\right)J_0 + (4\eta^2 + \bar{\sigma}^2)J_1\right],$$
$$g \equiv \frac{\sigma}{k_0}A\rho_1 + \frac{1}{k_0}J_1\rho_2 - H_2\Psi_r + \Psi\left(J_1 - \frac{\mu}{\sigma\eta}J_0\right), \tag{A.1}$$
$$h \equiv -\rho_3\bar{A} + \rho_4\bar{J}_1 + i\omega_0 Q\bar{\eta}SH_3 - \frac{1}{4}\Psi_r(\bar{\eta}\bar{J}_0 - \bar{J}_1) + \frac{\sigma\Psi}{4\Delta}[-\bar{\sigma}\bar{\eta}\bar{J}_0 + \sigma(i\bar{\sigma} - \bar{\eta}^2)\bar{J}_1].$$

In addition to each of the quantities σ, η, μ, Δ, J_m, N_m, A, H_1, H_2, H_3, ρ_1, ρ_2, ρ_3, ρ_4, f, g, and h there is another quantity denoted by the same letter with a bar above. The analytical equations connecting them remain current if each of the quantities without a bar (with a bar) is replaced by the quantity denoted by the same letter with a bar (without a bar) and the imaginary unit i is replaced by $-i$. We take $\sigma \equiv \sigma_1$; $\bar{\sigma} \equiv \sigma_{-1}$; $\eta \equiv \eta_1$; $\bar{\eta} \equiv \eta_{-1}$; $\Delta \equiv \Delta_1$; $\bar{\Delta} \equiv \Delta_{-1}$; $\mu \equiv \sigma + 2i$; $\Psi \equiv \Psi(k_0)$; $\Psi_r \equiv (d/d_r)\Psi(k_0 r)|_{r=1}$; $Q \equiv 2\pi k_0^2/(\sigma^2\bar{\sigma}^2)$; J_m and N_m are Bessel and Neumann functions of the argument η; J_m and $\bar{N}_m$ are those of the argument $\bar{\eta}$; $A \equiv (1/\Delta)(-\sigma\eta_0 + \sigma J_1)$;

$$H_1 \equiv \frac{4k_0^2}{\eta\sigma^3}rJ_0; \quad H_2 \equiv -\frac{\Delta}{\sigma^2\eta}rJ_0; \quad H_3 \equiv \Psi_r N_1 + \frac{\sigma\Psi}{\Delta}(-\sigma\eta N_0 + \bar{\sigma}N_1);$$
$$\rho_1 \equiv f_0(1) - \frac{M(b)I_1(k_0)}{k_0 I_1'(k_0 b)}; \quad \rho_2 \equiv M(1) - \frac{M(b)I_1'(k_0)}{I_1'(k_0 b)};$$
$$\rho_3 \equiv \frac{i}{2}\Psi + \frac{\sigma}{4}\left[\Psi_r + \frac{BF(b)I_1(k_0)}{k_0 I_1'(k_0 b)}\right]; \quad \rho_4 \equiv \frac{\sigma}{4\bar{\sigma}}\left[2F(1) - \frac{BF(1)I_1'(k_0)}{I_1'(k_0 b)}\right];$$
$$f_0(r) \equiv K_0(k_0 r) + \varkappa_1 I_0(k_0 r); \quad M(r) \equiv f_0(r) - k_0 r\Psi_0(k_0 r);$$
$$F(r) \equiv -\frac{r}{2}\Psi_{rr}(k_0 r) + \frac{1}{r}\Psi(k_0 r); \quad S \equiv \int_0^1 t^2 J_0(\bar{\eta}t)J_1(\eta t)\,dt.$$

For the principal points of intersection ($\omega_0 = 0$) the quantities k_0 are calculated from the equation

$$\Psi_r J_1 + (1/3)\Psi(\eta J_0 + J_1) = 0, \quad \eta = \sqrt{3}k_0.$$

The expressions for f and g follow from (A.1):

$$f = -\bar{f} = \frac{2i}{3}\left\{-2\eta J_0\Psi_r + \frac{1}{3}\Psi[(2\eta^2 + 1)J_1 - 2\eta J_0]\right\},$$
$$g = \bar{g} = \frac{\rho_1}{3k_0}(\eta J_0 + J_1) + \frac{\rho_2}{k_0}J_1 - \frac{3}{\eta}J_0\Psi_r + \left(J_1 - \frac{3}{\eta}J_0\right)\Psi.$$

At the same time, the quantity h in (A.1) does not yield the correct limit as $\omega_0 \to 0$. This is connected with the fact that important use is made of $\omega_0 \neq 0$ in the intermediate calculations. Separate calculations in which $\omega_0 = 0$ is taken from the very start yield

$$h = \overline{h} = \rho_5(\eta J_0 + J_1) + \rho_6 J_1 - (1/4)(3\eta J_0 - J_1)\Psi_r - (\eta/4)(J_0 - \eta J_1)\Psi,$$

$$\rho_5 \equiv \frac{1}{12}\left[2\Psi + \Psi_r + \frac{BF(b)\,I_1(k_0)}{k_0 I_1'(k_0 b)}\right], \quad \rho_6 \equiv -\frac{1}{2}\left[F(1) - \frac{BF(b)\,I_1'(k_0)}{2I_1'(k_0 b)}\right].$$

LITERATURE CITED

1. O. M. Phillips, The Dynamics of the Upper Ocean, 2nd ed., Cambridge Univ. Press, Cambridge—New York (1977).
2. C.-S. Yih, "Instability of surface and internal waves," Adv. Appl. Mech., 16, 369 (1976).
3. E. B. Gledzer, F. V. Dolzhanskii, et al., "Experimental and theoretical investigation of the stability of liquid motion inside an elliptical cylinder," Izv. Akad. Nauk SSSR, Fiz. Atmos. Okeana, 11, No. 10 (1975).
4. E. B. Gledzer, A. M. Obukhov, and V. M. Ponomarev, "Stability of liquid motion in vessels with an elliptical cross section," Izv. Akad. Nauk SSSR, Mekh. Zhidk. Gaza, No. 1 (1977).
5. C.-Y. Tsai and S. E. Widnall, "The stability of short waves on a straight vortex filament in a weak externally imposed strain field," J. Fluid Mech., 73, No. 4 (1976).
6. D. V. Moore and P. G. Saffman, "Structure of a line vortex in an imposed strain," in: Proceedings of the Symposium on Aircraft Wake Turbulence, Seattle, 1970, Plenum Press, New York (1971).
7. Lord Kelvin, "Vibrations of a columnar vortex," Philos. Mag., 10, 155 (1880).
8. V. A. Vladimirov, "Stability of flow of an ideal incompressible liquid with a constant vorticity in an elliptical cylinder," Zh. Prikl. Mekh. Tekh. Fiz., No. 4 (1983).

CONVECTIVE MOTIONS OF A FLUID IN A NEARLY SPHERICAL CAVITY WHEN HEATED FROM BELOW

Yu. K. Bratukhin and L. N. Maurin

UDC 531.529.2

1. It is known [1] that a nonuniformly heated fluid can be in mechanical equilibrium only if the temperature gradient in it is vertical and has a constant value. Such a situation can occur, for example, in a spherical cavity in a solid mass with a vertical (downward) temperature gradient specified at infinity.

Let us consider the effect of a nearly spherical cavity on convective stability. Suppose the equation of the surface of the cavity is $r = 1 + sP_2^{(1)} \cos\varphi$, where the $P_e^{(m)}(\vartheta)$ are associated Legendre polynomials, r, ϑ, φ are polar coordinates, the radius R_0 of the undeformed sphere is taken as unity, and $s \ll 1$. This special shape of the cavity was chosen since $P_2^{(1)} \cos\varphi$ is one of the large-scale spherical harmonics whose presence in the spectrum of functions specifying the shape of the actual cavity leads to distortion of the isotherms in the fluid, and consequently to convective motion for arbitrarily small temperature gradients.

We write the equations of steady-state convection in dimensionless form, choosing as units of velocity, pressure, and temperature $g\beta AR_0^3/\nu$, $\rho g\beta AR_0^2$, and AR_0 respectively, where ρ, β, and ν are respectively the density, coefficient of thermal expansion, and kinematic viscosity, $g = gk$ is the acceleration due to gravity, and $A = Ak$ is the constant temperature gradient at infinity. Then the equations and boundary conditions for the dimensionless velocity v, pressure p, and temperatures T_1 and T_2 in the solid mass in the fluid for steady-state motion take the form [1]

Perm. Ivanovo. Translated from Zhurnal Prikladnoi Mekhaniki i Tekhnicheskoi Fiziki, No. 3, pp. 69-72, May-June, 1983. Original article submitted March 30, 1982.